Theoretical Study of the Photothermal Behaviour of Self-Assembled Magnetic-Plasmonic Chain Structures

Kai Liu[a], Amir Mokhtare[b], Xiaozheng Xue[b], and Edward P. Furlani[a,b,*]

[a]Dept. of Electrical Engineering, University at Buffalo SUNY, NY 14260

[b]Dept. of Chemical and Biological Engineering, University at Buffalo SUNY, NY 14260.

[*]E-mail : efurlani@buffalo.edu

Monte Carlo based Computational Method:

In the Monte Carlo analysis, we assume that the Fe_3O_4 material has a saturation magnetization $M_{sp} = 4.78\times10^5$ A/m and that the applied external field is $H_a = 3.9\times10^5$ A/m ($B_a = 5000$ Gauss), which can be provided by rare-earth permanent magnets and is sufficiently strong to saturate the nanoparticles considered in our study. To simplify the analysis, the carrier fluid is assumed to be nonmagnetic ($\chi_f = 0$). Simulations were performed using the Monte Carlo method with the Metropolis algorithm to determine the final equilibrium particle structures. The approach was as follows. First, an initial configuration is generated consisting of randomly distributed particles. Each particle is then subjected to a random walk with a limited displacement step to generate a new position $(x_{new}, y_{new}, z_{new})$ in the particle trail. The change in the total energy ΔU between new and initial configurations is then evaluated based on the particle displacement. The total energy U includes the magnetostatic and magnetic dipole-dipole energies, electrostatic energy, Van der Waals potential energy and a surfactant energy that is computed when the particles are in contact. A uniform random number δ is generated with $0 < \delta < 1$ and if it meets the expression:

$$\delta < \exp\left(-\frac{\Delta U}{k_B T}\right) \qquad \text{(S1)}$$

, the particle displacement is accepted and the new particle configuration is adopted. This process is repeated until equilibrium is reached. Our computational model takes into account several dominant assembly mechanisms, including the induced magnetostatic, magnetic dipole-dipole interactions, the electrostatic repulsion, Brownian dynamics, Van der Waals interaction and a steric repulsive force caused by surfactant-surfactant contact, which are described as follows.

Interaction with an Applied Magnetostatic Field: The magnetostatic energy is predicted using an "effective" dipole moment method in which the particle is modeled as an "equivalent" point dipole with an effective moment. The moment is defined by $\boldsymbol{m}_{eff,i} = V_{p,i} M_p$, where $V_{p,i}$ and M_p is the volume and magnetization of the particle i, respectively. For magnetic-dielectric core-shell particles, only the core contributes to that magnetic force and consequently, $\boldsymbol{m}_{eff,i} = V_{core,i} M_p$. The moment can be determined using a magnetization model that takes into account self-demagnetization and magnetic saturation of the particles.

$$\boldsymbol{m}_{i,eff} = V_{core,i} f\left(H_a\right) \boldsymbol{H}_a \qquad \text{(S2)}$$

, where

$$f\left(H_a\right) = \begin{cases} \dfrac{3\left(\chi_p - \chi_f\right)}{\left(\chi_p + 2\chi_f\right)+3} & H_a < \left(\dfrac{\left(\chi_p + 2\chi_f\right)+3}{3\left(\chi_p - \chi_f\right)}\right) M_{sp} \\ M_{sp} / H_a & H_a \geq \left(\dfrac{\left(\chi_p + 2\chi_f\right)+3}{3\left(\chi_p - \chi_f\right)}\right) M_{sp} \end{cases} \qquad \text{(S3)}$$

In this expression, χ_f is the susceptibility of the carrier fluid, M_{sp} is the saturation magnetization of the particle, and χ_p is its intrinsic magnetic susceptibility. The magnetic potential energy U_m of the i'th particle is given by

$$U_{m,i} = -\boldsymbol{m}_{eff,i} \cdot \boldsymbol{B}_a \qquad \text{(S4)}$$

The force on the particle is obtained by taking the gradient of the magnetostatic energy.

Magnetic Dipole-dipole Interactions: A potential energy U_{dd} due to the magnetic dipole-dipole interaction can be described as the following equation,

$$U_{dd,ij} = -\frac{\mu_f}{4\pi}\left(3\frac{\left(\boldsymbol{m}_{i,eff} \cdot \boldsymbol{r}_{ij}\right)\left(\boldsymbol{m}_{j,eff} \cdot \boldsymbol{r}_{ij}\right)}{r_{ij}^5} - \frac{\boldsymbol{m}_{i,eff} \cdot \boldsymbol{m}_{j,eff}}{r_{ij}^3}\right) \qquad \text{(S5)}$$

, where $\boldsymbol{m}_{eff,i}$ and $\boldsymbol{m}_{eff,j}$ are the moments of i'th and j'th particle, respectively, and $\boldsymbol{r}_{ij}$ is the displacement vector between them. Note that $U_{dd,ij} \propto R_{core}^6$ for identical core shell particles.

Interparticle Electrostatic Interactions: The electrostatic repulsion between particles due to the double layer forces is described by the DLVO theory. An electrostatic energy U_e is generated by,

$$U_{e,ij} = -2\pi\varepsilon\varepsilon_0\left(\frac{k_B T}{ze}\right)^2 R_p q^2 \ln\left(1 - e^{-\kappa h_{ij}}\right) \qquad \text{(S6)}$$

, where ε is relative permittivity, ε_0 is the permittivity of free space, z is the valency of ions, e is the fundamental electronic charge, κ^{-1} is the Debye decay length, n_b is the concentration of ions, q is the surface charge.

Van der Waals Potential Energy: Van der Waals potential Energy is calculated using

$$U_{v,ij} = -\frac{A}{6}\left(\frac{2R_{p,i}R_{p,\mathrm{j}}}{r_{ij}^2 - \left(R_{p,i} + R_{p,j}\right)^2} + \frac{2R_{p,i}R_{p,\mathrm{j}}}{r_{ij}^2 - \left(R_{p,i} - R_{p,j}\right)^2} + \ln\frac{r_{ij}^2 - \left(R_{p,i} + R_{p,j}\right)^2}{r_{ij}^2 - \left(R_{p,i} - R_{p,j}\right)^2}\right) \qquad \text{(S7)}$$

, where A is the Hamaker constant, $R_{p,i}$ and $R_{p,j}$ are the radius of the i'th and j'th particle, respectively.

Surfactant Interaction: A potential energy U_s is introduced into our model due to the surfactant-surfactant contact, which is used to preclude particle overlapping during assembly,

$$U_{s,ij} = 2\pi \frac{R_{p,i}^2 \cdot R_{p,\mathrm{j}}^2}{(R_{p,i} + R_{p,j})^2} N_s k_B T \left\{ 2 - \frac{r_{ij} - (R_{p,i} + R_{p,j})}{\bar{\delta}} - \frac{r_{ij}}{\bar{\delta}} \ln\left(\frac{(R_{p,i} + R_{p,j}) + 2\bar{\delta}}{r_{ij}}\right) \right\} \quad \text{(S8)}$$

, where $\bar{\delta}$ and N_s are the average thickness of the surfactant layer and the surface density of surfactant molecules, respectively.

Viscous Drag: The drag force on a particle is computed using Stokes' formula

$$\boldsymbol{F}_{\mathrm{vis},i} = D_i \frac{d\boldsymbol{x}_i}{dt} \quad \text{(S9)}$$

, where $D_i = 6\pi\eta R_{hyd,p,i}$ is described as the drag coefficient (η is the fluid viscosity and $R_{hyd,p,i}$ is the hydrodynamic radius of the i'th particle).

Interparticle Hydrodynamic Interactions: Hydrodynamic interactions between particles become important at small surface-to-surface separation distances. The force between two neighboring particles is based on lubrication theory and given by,

$$\boldsymbol{F}_{hyd,ij} = \frac{6\pi\eta \boldsymbol{V}_{r,i,j}}{h_{ij}} \frac{R_{p,i}^2 R_{p,j}^2}{\left(R_{p,i} + R_{p.j}\right)^2} \quad \text{(S10)}$$

, where h_{ij} is the separation between the surfaces and $\boldsymbol{V}_{r,i,j}$ is the relative velocity between the particles. When the particles are in contact ($h_{ij} \le 0$) this force is considered to be negligible.

Brownian Motion: The Brownian force in one dimension is modeled as a Gaussian white noise process

$$F_{B,i} = \xi \sqrt{\frac{2D_i k_B T}{\Delta t}} \quad \text{(S11)}$$

, where k_B is Boltzmann's constant, D_i is the Stokes' drag coefficient as described above and ξ is a random number with a Gaussian distribution. The 3D Brownian force is obtained by applying this equation for each force component.

Finite Element based Computational Method:

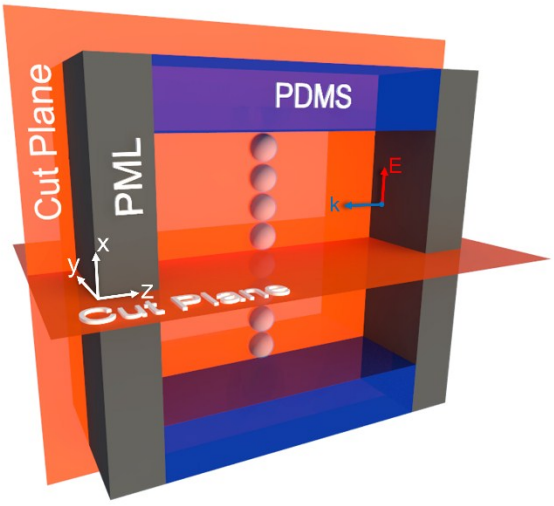

Figure S1. The computational domain for optical property calculation.

We used 3D full-wave computational models to study the optical behaviors of magnetic-plasmonic chains. Specifically, we used the finite element (FE)-based Radio Frequency (RF) solver module in the commercial COMSOL multiphysics program (COMSOL Version 5.3, www.comsol.com). The dimensions of individual nanoparticles are identical to those employed in the self-assembly analysis. A 3D computational photonic analysis is employed to investigate the optical properties in the 1D chain of Fe_3O_4@Au nanoparticles. The computational model is well defined in a Cartesian coordinate (x, y, z). The chain is illuminated with a uniform plane wave with the E field parallel to the x-axis which is identical to the direction of 1D chain. A surface current boundary is employed as the excitation source.

Fig. S1 shows the full model consisting of PDMS layers (blue) for channel formation, perfect matched layers (PMLs, grey) for backscattering elimination, and water environment wrapping around the single chain. The chain is illuminated with a uniform plane wave with the E field parallel to the x-axis which is identical to the direction of 1D chain. The wave will propagate along the negative direction of the z-axis which is indicated by the wave vector **k** in **Fig. S1**. A surface current boundary is employed as the excitation source, as shown in the literature[1-3]. In order to reduce the computation time and required computer resources, the final computational model is obtained by cutting the full model into a quarter along the symmetric planes (orange). Perfect electric conductor (PEC) conditions are applied at the boundries perpendicular to **E**, and perfect magnetic conductor (PMC) conditions are applied at the boundries perpendicular to **H**. It is important to note that these symmetry BCs mimic the response of an infinite 2D array of chains with a center-to-center *x* and *y* lattice spacing equal to the spatial period of the CD.

The time-harmonic E field within the domain satisfies the equation:

$$\nabla \times \left(\mu_r^{-1} \nabla \times \mathbf{E}\right) - k_0^2 \left(\varepsilon_r - j\frac{\sigma}{\omega \varepsilon_0}\right)\mathbf{E} = 0 \qquad \text{(S12)}$$

where μ_r, ε_r and σ are the relative permeability, permittivity and conductivity of the media, respectively. In the computational model, we compute the power absorbed by the particle Q_{abs} (W) and then use this to compute the cross section $\sigma_{abs} = Q_{abs}/I_{laser}$, where I_{laser} (W/m^2) is the incident irradiance.

Material Properties:

The refractive index of the surrounding medium ($n_m = n_{H_2O}$), in this case H_2O, is also assumed to be lossless[4], i. e.

$$n_{H_2O}^2 = 1 + \frac{0.5684027565\lambda^2}{\lambda^2 - 0.005101829712} + \frac{0.1726177391\lambda^2}{\lambda^2 - 0.01821153936} + \frac{0.02086189678\lambda^2}{\lambda^2 - 0.02620722293} + \frac{0.1130748688\lambda^2}{\lambda^2 - 10.69792721} \qquad \text{(S13)}$$

In these expressions λ is the vacuum wavelength in units of micrometers.

Gold: When the gold shells are thinner than the mean free path of the free electrons (~ 42 nm), a dielectric function for gold that accounts for electron-surface scattering is described as[4]

$$\varepsilon_{Au}\left(\omega, L_{eff}\right) = \varepsilon_{Au,bulk}\left(\omega\right) + \frac{\omega_p^2}{\omega^2 + i\omega v_f / l_\infty} - \frac{\omega_p^2}{\omega^2 + i\omega(v_f / l_\infty + A v_f / L_{eff})} \qquad \text{(S14)}$$

, where $\varepsilon_{Au,bulk}$ is the bulk dielectric function of gold, ω is the angular frequency of incident light, $\omega_p = 0.93$ eV is the plasma frequency, $v_f = 1.40 \times 10^{15}$ nm/s is the Fermi velocity, $l_\infty = 42$ nm is the mean free path of the free electrons, A is a dimensionless parameter, usually assumed to be

close to unity ($A=1$) and $L_{eff}=\frac{D_p-D_c}{2}$ is the reduced effective mean free path of the free electrons. The bulk dielectric function is given by an analytical expression that is based on an experiment-fitted critical points model[5-7],

$$\varepsilon_{Au,bulk}(\lambda)=\varepsilon_{\infty}-\frac{1}{\lambda_p^2\left(\frac{1}{\lambda^2}-i\frac{1}{\gamma_p\lambda}\right)} + \sum_{n=1,2}\frac{A_n}{\lambda_n}\left[\frac{e^{i\phi_n}}{\left(\frac{1}{\lambda_n}-\frac{1}{\lambda}+i\frac{1}{\gamma_n}\right)}+\frac{e^{-i\phi_n}}{\left(\frac{1}{\lambda_n}+\frac{1}{\lambda}-i\frac{1}{\gamma_n}\right)}\right]. \quad \text{(S15)}$$

Fe_3O_4: The Fe_3O_4 core is lossy and the refractive index of Fe_3O_4 at optical frequencies has not been widely reported. We obtain values for the real and imaginary components of $n_{Fe_3O_4}$ in tabular form by discretizing plots of measured data found in the literature[8]. As noted, since $n_{Fe_3O_4}$ is complex-valued the core contributes to absorption in the Fe_3O_4@Au NPs.

Thermodynamic Model:

The thermodynamic model is based on the same computational domain as the photonic analysis except that a thermal insulation condition is imposed on all boundaries. The temperature T throughout the computational domain satisfies the equation,

$$\rho C_p\frac{\partial T}{\partial t}+\nabla\cdot(-k\nabla T)=Q \qquad \text{(S16)}$$

, where Q (W/m^3) is the thermal energy generated per unit volume, i.e. Q=Q_h inside the gold shell and Fe_3O_4 core, and Q = 0 in all other (loss less) materials. Here, ρ is the density, C_p is the specific capacity and k is the thermal conductivity of the material. In our analysis, the temperature-dependent thermal conductivity, heat capacity, and material density of the surfactant (assumed to be polymer), gold, Fe_3O_4, and water are extracted from the previous literatures[9-13]. The initial temperature is set to 20 °C.s

References

1. Alali, F.; Kim, Y. H.; Baev, A.; Furlani, E. P., Plasmon-Enhanced Metasurfaces for Controlling Optical Polarization. *ACS Photonics* **2014**, *1*, 507-515.
2. Furlani, E. P.; Baev, A., Free-Space Excitation of Resonant Cavities Formed from Cloaking Metamaterial. *J. Mod. Opt.* **2009**, *56*, 523-529.
3. Furlani, E. P.; Baev, A., Optical Nanotrapping Using Cloaking Metamaterial. *Phys. Rev. E* **2009**, *79*.
4. Tuersun, P.; Han, X., Optical Absorption Analysis and Optimization of Gold Nanoshells. *Appl. Opt.* **2013**, *52*, 1325-1329.s
5. Johnson, P. B.; Christy, R. W., Optical Constants of the Noble Metals. *Phys. Rev. B* **1972**, 4370-4379.
6. Etchegoin, P. G.; Le Ru, E. C.; Meyer, M., Erratum: "An Analytic Model for the Optical Properties of Gold" [J. Chem. Phys. 125 , 164705 (2006)]. *J. Chem. Phys.* **2007**, *127*, 189901.
7. Etchegoin, P. G.; Le Ru, E. C.; Meyer, M., An Analytic Model for the Optical Properties of Gold. *J. Chem. Phys.* **2006**, *125*, 164705.

8. Schlegel, A.; Alvarado, S. F.; Wachter, P., Optical Properties of Magnetite (Fe_3O_4). *J. Phys. C: Solid State Phys.* **1979**, *12*, 1157-1164.s
9. Gaur, U.; Wunderlich, B., Heat-Capacity and Other Thermodynamic Properties of Linear Macromolecules .5. Polystyrene. *J. Phys. Chem. Reference Data* **1982**, *11*, 313-325.
10. Takeda, M.; Onishi, T.; Nakakubo, S.; Fujimoto, S., Physical Properties of Iron-Oxide Scales on Si-Containing Steels at High Temperature. *Mater. Trans.* **2009**, *50*, 2242-2246.
11. Gronvold, F.; Sveen, A., Heat-Capacity and Thermodynamic Properties of Synthetic Magnetite (Fe3o4) from 300 to 1050 K - Ferrimagnetic Transition and Zero-Point Entropy. *J. Chem. Thermodyn.* **1974**, *6*, 859-872.
12. Skelskey, D.; Vandensy.J, High Temperature Specific Heat of Gold Using Modulation Method. *J. Appl. Phys.* **1970**, *41*, 4750.
13. Chase, M. W., Jr., Nist-Janaf Themochemical Tables, Fourth Edition. *J. Phys. Chem. Ref. Data* **1998**, *Monograph 9*, 1-1951.